Large eddy simulation of unsteady turbulent flow in a semi-industrial size spray dryer

F. Jongsma, F. Innings, M. Olsson, F. Carlsson

Dairy Sci. & Technol. (2013) 93:373–386
DOI 10.1007/s13594-012-0097-y

ORIGINAL PAPER

Large eddy simulation of unsteady turbulent flow in a semi-industrial size spray dryer

F. J. Jongsma · F. Innings · M. Olsson · F. Carlsson

Received: 23 September 2012 / Revised: 4 December 2012 / Accepted: 4 December 2012 /
Published online: 10 January 2012

Abstract This paper is concerned with the numerical simulation of gas flow inside spray dryers, which is known to be highly transient. Experimental evidence presented in the literature to date is acquired either at a scale much smaller than industrial or at a limited number of locations in the system (e.g. the central axis). Alternatively, computational fluid dynamics (CFD) simulation, in particular methods based on the Reynolds-averaged Navier–Stokes (RANS) equations, may provide the information of the complete flow field at industrial scales. However, RANS methods to some extent are hampered by the limitations of turbulence modelling. In this study, it has been investigated whether the current limitations of experiments and RANS CFD simulations can be omitted by the use of large eddy simulation (LES). The spray dryer studied was of semi-industrial size with a volume of 60 m^3. Via grid size and time step refinement studies, the minimum numerical requirements for obtaining converged time averaged velocity profiles could be identified. Spectral analysis and estimates of the Kolmogorov scales demonstrated that LES resolves scales well into the inertial subrange of turbulence scales. The LES calculation shows a complex precession of the jet. The jet moves around in the drying chamber seemingly with no reoccurring modes. Even with very long sampling times, no typical frequencies could be found. This work demonstrates the feasibility of LES for a spray dryer of semi-industrial scale and the ability of LES to predict large-scale motions. Future work will include the further validation of the LES via comparison with laser Doppler anemometry measurements and, subsequently, the comparison of RANS, unsteady RANS and LES simulations.

Keywords LES · CFD · Spray dryer · Transient flow

F. J. Jongsma (✉)
Tetra Pak CPS, Venus 100, 8448 GW Heerenveen, The Netherlands
e-mail: alfred.jongsma@tetrapak.com

F. Innings
Tetra Pak Processing Systems, Ruben Rausings Gata, 221-86 Lund, Sweden

M. Olsson · F. Carlsson
Tetra Pak Packaging Solutions, Ruben Rausings Gata, 221-86 Lund, Sweden

1 Introduction

Computational fluid dynamics (CFD) simulation of the spray drying process has received considerable attention, both in academia and industry, since the value of modelling as an aid in design of new systems, exploration of what-if scenarios or troubleshooting studies (Fletcher et al. 2006) is recognised. In contrast to the deceptively simple appearance of the technology, the physical processes taking place inside the spray dryer are numerous, complex and highly coupled. In the present paper, some of the complexities of the air phase flow will be addressed.

The air flow inside spray dryers may be characterised as confined jet flow. Several investigators (Usui et al. 1985; Kieviet et al. 1997; Godijn et al. 1999; Woo et al. 2009) have observed the confined jet may exhibit transient, large-scale motions. The term 'large' here refers to the order of magnitude of the spray dryer itself. For example, the jet emanating from a central inlet in the roof of a spray dryer may deflect from the central axis towards the wall, and it may precess around the central axis. In contrast, the average velocity field of a free jet is axisymmetric and will exhibit steady-state behaviour. Once the jet is confined by walls, small deviations of the jet from the central axis may grow, in a self-sustained manner, and in turn continue to deflect the jet (Guo et al. 1998).

The observed transient flow patterns of the confined jet depend on: extent of swirl in the inlet flow (Southwell and Langrish 2001; Guo et al. 2001a), the Reynolds number of the jet (Guo et al. 2001b) and the geometrical features of the system (Guo et al. 2001a, b, c). A map of flow regimes was presented by Guo et al. (2001b). The regimes identified were termed, steady, transition, regular precession and complex precession. The term steady refers to a flow regime closely resembling that of the free jet, but now with a stable toroidal flow structure around it. The steady regime is encountered when the walls are close to the jet, or expressed differently when the expansion ratio, defined as the ratio of system and inlet diameters, is small. Upon increasing the expansion ratio, a transitional regime may be observed before regular precession is encountered. Moving the walls even further away from the central axis will result in a regime change from regular to complex precession. In the latter regime, the precession is no longer of constant amplitude and frequency but chaotic instead.

Early attempts to simulate the spray drying process were usually based on the assumptions of steady-state behaviour and axial symmetry, allowing for the use of computationally less expensive 2D geometries. Currently, it is being acknowledged (Fletcher et al. 2006) that the predictive power of the CFD simulation of spray dryers will benefit from considering full 3D geometries and transient simulations. Modelling efforts thus far have almost exclusively relied on solving the RANS equations in conjunction with the well known k-ε or k-ω based turbulence models. One exception was reported by Fletcher and Langrish (2009), who applied the scale adaptive simulation approach to the simulation of a pilot spray dryer. It appears that the approaches that rely less on turbulence modelling, such as detached eddy simulation and large eddy simulation (LES) have not been explored yet.

Most experimental observations have been made on simple geometric systems (Dellenback et al. 1988, Hallet et al. 1984), e.g. a sudden expansion, or on spray dryers of laboratory size, up to spray dryers of approximately 1 m in diameter. Industrial spray dryers, especially for milk powder production, are usually an order of magnitude bigger and consequently are operated at higher Reynolds numbers. The

goal of this work is to investigate the flow features of a system that is closer to an industrial size. Given the decrease in cost of computing power LES has been used. The present report is aimed firstly at demonstrating the feasibility of LES simulation of a spray dryer of semi-industrial scale and secondly at an initial exploration of large scale features of the flow in this system. Future work will include further validation of the LES model results by comparison with measured data.

2 Methods

2.1 System

The spray dryer studied is presented in Fig. 1. The pilot spray dryer is of the cylinder on cone type, with cylindrical dimensions of 3.8 m diameter and 4.1 m height and a cone top angle of 43°, resulting in a total volume of 60 m^3. Air is fed through an annular gap in the roof and it escapes the dryer through four top outlets. The inlet is annular due to the fact that a pipe with a diameter of 0.103 m is located on the vertical axis of the dryer where normally fine powder is fed for the purpose of agglomeration. The inlet diameter of the dryer is 0.437 m and the expansion ratio 8.7. For the simulations, the outlets were simplified as indicated in Fig. 1. The Reynolds number of the jet, based on a feed rate of 6,440 kg h^{-1} and the air inlet diameter was 5.10^5.

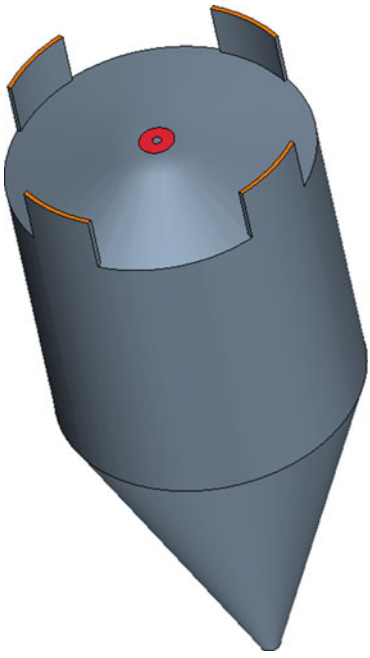

Fig. 1 Pilot Tetra Pak-wide body spray dryer

2.2 Simulation set-up and procedure

For the simulations, the commercially available package Fluent 13.0.0 was used while post processing was more conveniently handled in StarCCM+ and Python. Details of the simulation set-up have been presented in Table 1. Initial velocity and pressure fields for the LES simulation where obtained by steady-state RANS calculations, using the k-ε RNG turbulence model. Also, the velocity inlet profile for the spray dryer was determined by the use of a RANS simulation of the inlet system.

A well-resolved LES simulation is ensured by using sufficiently small time steps and cell sizes. The cell size determines the spatial cut-off between the resolved and unresolved scales. To ensure that the large scales are indeed resolved the cut-off should be chosen such that it falls into the universal equilibrium range of the turbulence energy spectrum. A sufficiently small time step allows the temporal resolution of the large scales. Davidson (2010) has reported on the quality of several methods to assess the resolution of LES simulations and concludes that two point correlation methods are preferred over analysis of energy spectra, dissipation energy spectra or ratios of resolved and unresolved quantities like shear stress. However, given that LES simulations still are time consuming and that the methods proposed in literature assess the resolution during or at the end of the simulation, here a more practical approach was adopted.

Table 1 Simulation set-up

Turbulence model	LES, dynamic Smagorinsky
Material	Air, incompressible 25 °C
Numerical details	
Pressure–velocity coupling	Fractional step
Momentum	Bounded central differencing
Pressure	Standard
Gradients	Least squares cell based
Time	Bounded second order implicit
Boundary conditions	
Inlet	Velocity obtained from RANS (Vortex method)
Outlets	Pressure, ambient
Mesh sizes	
Very coarse	~1.10^6 cells
Coarse	~7.10^6 cells
Fine	~24.10^6 cells
Simulation parameters	
Total simulation time	80–190 s
Start data sampling	40 s
Time step	0.12–0.5 ms
Courant number	~1, in all simulations

To allow for sufficiently small residuals, proper convergence was ensured in several ways. Firstly, the courant number of the calculations was kept below (but close) to one. Secondly, three combinations of grid size and time step refinements were tested to ensure independency on both parameters. Finally, the grid cell and time step sizes where compared with estimates of the Kolmogorov scales of turbulence obtained from the steady state RANS simulations. Estimates of the Kolmogorov scales are obtained from RANS simulations, via the turbulence energy dissipation rate, ε. Their significance with respect to the judgement of the resolution will be explained below.

2.3 Data sampling, treatment and interpretation

During the simulations, velocity and pressure data were stored at every time step for 54 monitoring points at locations sketched in Fig. 2. The axes shown in the bottom left corner of Fig. 2 indicate the chosen Cartesian frame of reference. Throughout this text, it is understood that u, v and w represent the velocity components in the respective directions x, y and z. For visual comparison and animation purposes, velocity and pressure data were stored at a rate of 25Hz for the planes: $x=0$, $y=0$, $z \in [-1.6, -3.3, -4.6]$. Average field data of the entire domain could be obtained from the simulation software directly.

The velocity data gathered for the 54 monitoring points was analysed statistically, mainly for the purpose of future comparison to results of laser Doppler

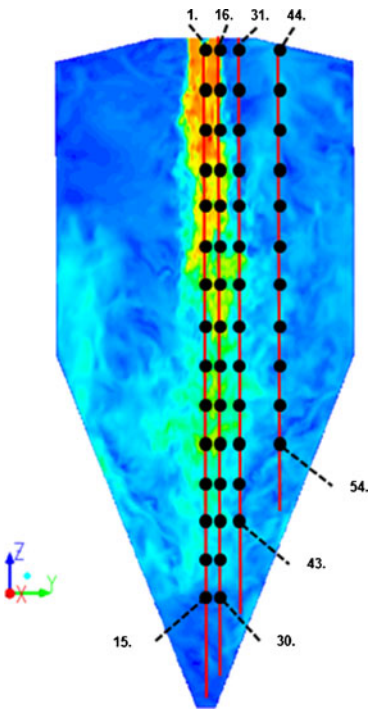

Fig. 2 Locations and numbering of monitor points on the plane $x=0$

anemometry measurements. The individual point velocity–time signals obtained were subjected to Fourier transformation for the construction of power spectral densities (PSD), to reveal possible dominant frequencies associated with certain scales of the turbulent structures.

Further investigation of flow patterns was conducted by applying a low-pass filter to the frequency signal of the velocity fluctuations, u', v' and w'. The velocity fluctuations were obtained by subtracting the average from the actual velocity. The time signal of the velocity fluctuation was then reconstructed from the Fourier components of the low frequencies. For several points, the filtered cross-sectional (u', v') velocity fluctuations where plotted in the form of a so-called phase space plot. A similar method was proposed earlier by Guo et al. (2001b, 2003) for the identification of periodicity in the results of transient RANS simulations.

Compared with the case of interpreting results of transient RANS calculations, here a choice needs to be made on the frequency that is used for filtering. Depending on the exact choice, different patterns may arise in the phase space plot making direct comparison troublesome. The significance of the phase space plot however lies more in the fact whether or not patterns that may appear are regular or not. Hence, regardless of the exact choice of filtering frequency, phase space plots will reveal either periodicity or irregularity.

3 Results and discussion

3.1 Visualisation of the flow field

Contour plots of the instantaneous velocity field (Fig. 3) demonstrated the time-dependent motions in the flow field. Detectable motions of the flow ranged from roll-up vortices, typical for the shear layer of the jet, up to more complex movements of the entire jet.

Visual inspection of animations, constructed from the contour plots of the horizontal planes ($z\in$ [−1.6, −3.3, and −4.6]), revealed a gradual breakdown of the jet structure upon deeper entering the dryer. At a height of −1.6 m, the jet was still located centrally in the dryer, circular in shape and nearly invariant in axial velocity. Deeper into the spray dryer, e.g. z=−4.6, the shape of the jet was observed to be stretched, deflected from the central axis and no longer exhibited a spatially flat velocity profile, see Fig. 3. Large-scale motions in the space surrounding the jet could be observed in animations constructed from the contour plots of the vertical planes. It appeared that movement of the jet towards the wall was often accompanied by strong gusts of flow on the opposite wall. These gusts of higher upward velocity started at approximately half the height of the cone and could extend as far as up to the roof of the dryer. In Fig. 4, one example of the observed gusts is presented as combined contour (w) and vector plot, indicating the instantaneous velocities.

The structure of the turbulence was visualised by iso-surfaces of the Q criterion as shown in Fig. 5. The Q criterion is a scalar quantity that is defined as $Q=0.5\cdot(\Omega^2-S^2)$, where Ω is the vorticity magnitude and S the mean strain rate. If at a certain location

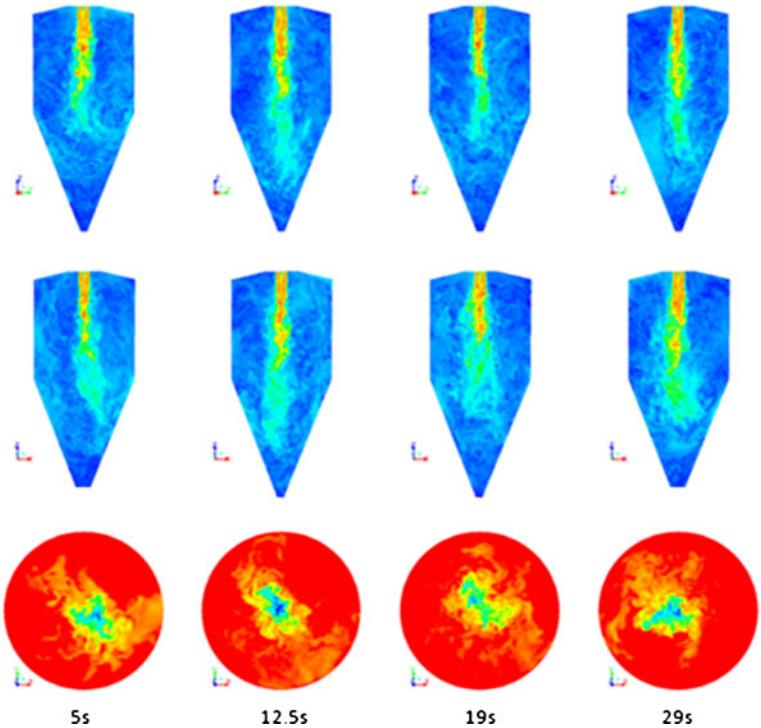

Fig. 3 Contour plots of velocity magnitude (*top*, *middle*) and axial velocity components, *w*, (*bottom*) for the planes: $x=0$ (*top*), $y=0$ (*middle*) and $z=-4.6$ (*bottom*), at times counted from the start of data collection (i.e. $t>40$ s)

in the flow the Q criterion is positive, this indicates that the rotation dominates the strain and shear.

The time-averaged velocity magnitude and the turbulence kinetic energy fields, shown in Figs. 6 and 7, respectively, appeared to be symmetric. The symmetry of both fields is an indication that the total simulation time was several times more than the time-scale of transient flow structures.

The contour plot of the average velocity field (Fig. 6) further supported the observations made from the animations that there are frequent gusts of upward flow alongside the walls. Inside the conical section, the average flow field of the jet is directly surrounded by an area of low average velocity, which in turn is surrounded by an area of higher, upward velocity.

3.2 Convergence tests

In Fig. 8, the downward directed, axial velocity component *w*, is plotted as a function of dimensionless axial distance (based on inlet diameter) for the three combinations of cell and time step sizes. To avoid repetition similar plots, e.g. the radial velocity profiles, are omitted. It was noted, however, that the (time averaged) LES solution indeed converged upon cell size and time step refinement.

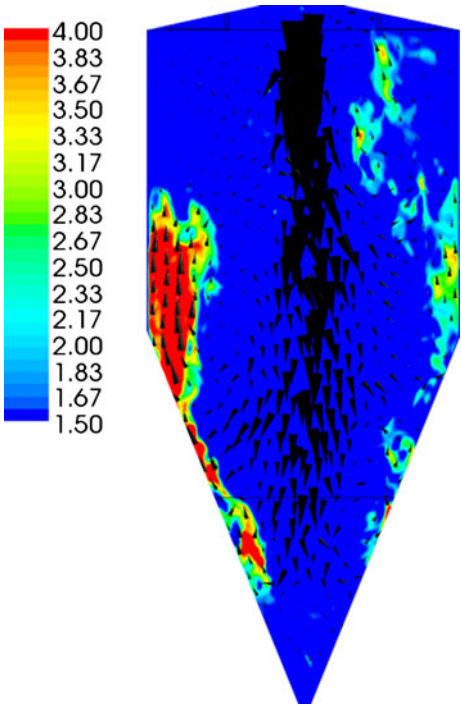

Fig. 4 Contour plot of instantaneous axial velocity w (metres per second) and vectors, plane $x=0$

Estimates of the Kolmogorov length and time scales, obtained from steady-state RANS simulations, were divided by, respectively, the cell and time step sizes. Figures 9 and 10 contain the contour plots of the ratios thus obtained, for the case of smallest cell size and time step.

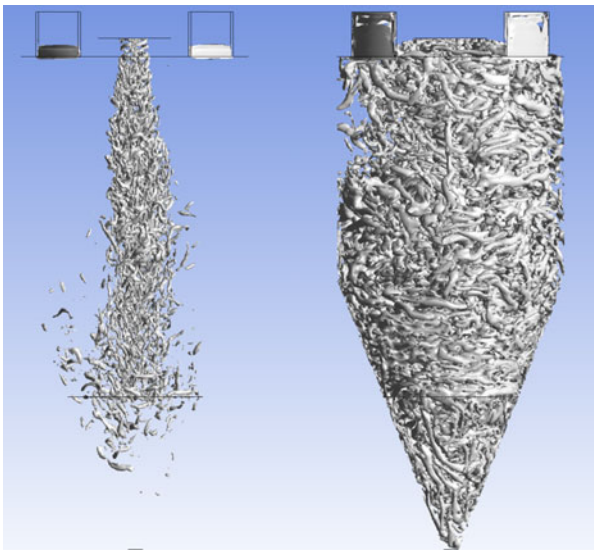

Fig. 5 Isosurfaces of the Q criterion: *left* $Q=0.04$, *right* $Q=0.005$

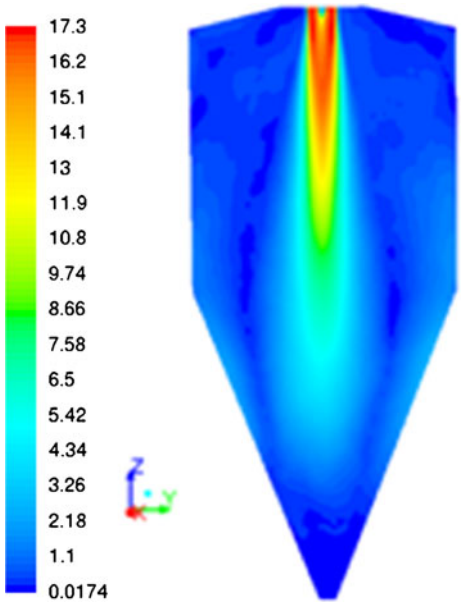

Fig. 6 Contour plot of average velocity magnitude (metres per second) plane $x=0$

From Fig. 9, it appeared that the cell size used is approximately between 40 and 100 times larger than the Kolmogorov length-scale estimate. For sufficient spatial resolution of the LES simulation it is required that the cell size is similar to that of the size of eddies in the universal equilibrium range. The Taylor length scale, λ, representing the length scale in the inertial subrange of the universal equilibrium range, was used to check this requirement. The ratio

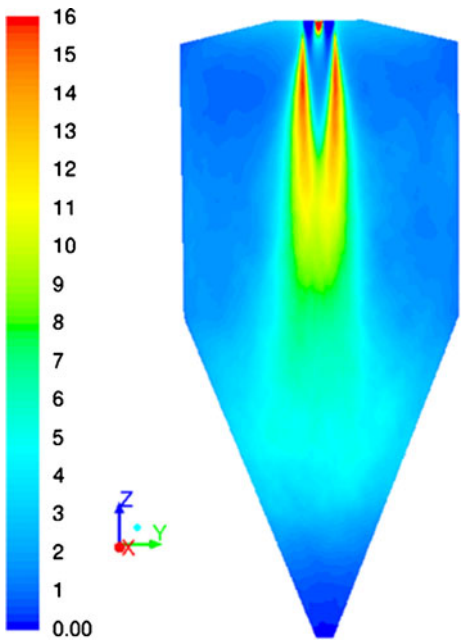

Fig. 7 Contour plot of turbulence kinetic energy (Joules per kilogramme) plane $x=0$

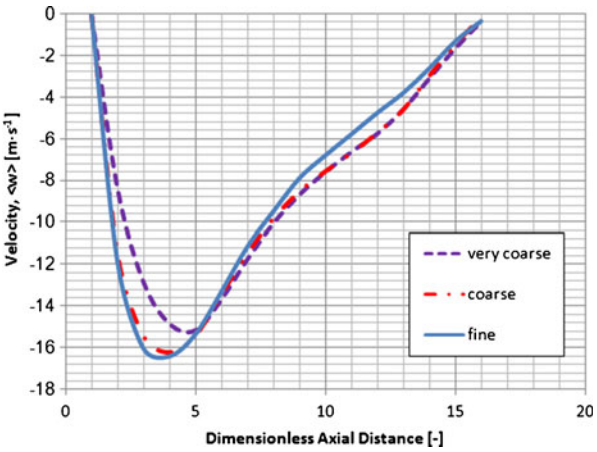

Fig. 8 Averaged centre-line velocity in the vertical direction plotted versus dimensionless distance in the dryer

of the Taylor length scale and the Kolmogorov length scale, η, is related to the Reynolds number of turbulence, Re_L, as:

$$\frac{\lambda}{\eta} = \sqrt{10}(Re_L)^{1/4}$$

The Reynolds number of turbulence is defined as:

$$Re_L = \frac{k^2}{\varepsilon \cdot \nu}$$

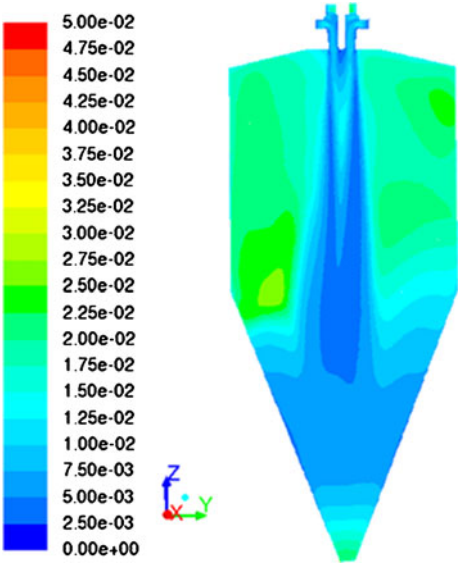

Fig 9 Contour plot of Kolmogorov length-scale estimate divided by grid cell size

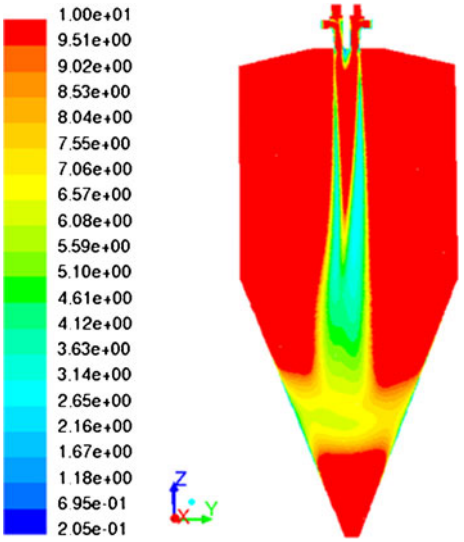

Fig. 10 Contour plot of Kolmogorov time-scale estimate divided by time step size

where k represents the turbulence kinetic energy and ν the kinematic viscosity. The Reynolds number of turbulence, also obtained from RANS simulation, was observed to vary between 10^3 around the jet and 10^5 inside the jet. The ratio of λ/η therefore varied between 32 and 56. The cell size thus appeared to be close to the size of the Taylor length scale.

Figure 10 demonstrated that the time step used is at worst approximately equal to the Kolmogorov time-scale estimate and at best ten times smaller. It may therefore be concluded that the temporal resolution is sufficient.

3.3 Large-scale motions

The sampled velocity data were subjected to spectral analyses. Figures 11 and 12 below show the resulting PSD for the axial velocity component for several locations inside the dryer. In Figs. 11 and 12, only the frequency content below

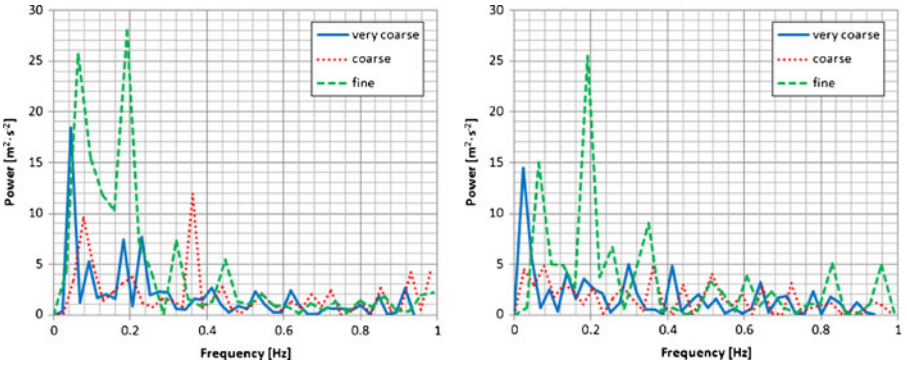

Fig. 11 Power spectra (w') of point 19 (*left*) and point 24 (*right*). Point locations as indicated in Fig. 2

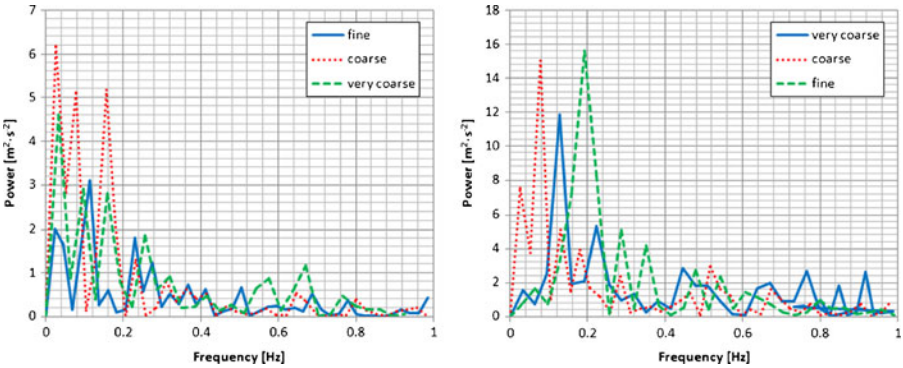

Fig. 12 Power spectra (w') of point 47 (*left*) and point 52 (*right*). Point locations as indicated in Fig. 2

1Hz is shown because the large-scale motions are moving slow compared with smaller scales of turbulence, and hence end up as low frequencies in the PSD. PSD plots were constructed for all the monitoring points and all velocity components. In all cases, similar behaviour was encountered; there appeared to be maxima in the low frequency range, but a single dominant frequency could not be detected.

In Fig. 13, low pass-filtered velocity fluctuations were plotted against time for point 19. The filtered velocity signal shows fluctuations of the velocity that have a magnitude up to 40% of the average velocity.

Though the results of Fig. 13 show that the flow is transient in nature, the motions of the flow do not seem to be regular. A phase space plot of the low-pass filtered (0.5 Hz) cross-sectional velocities at the same point (Fig. 14) further confirmed this observation. The behaviour as depicted in Figs. 13 and 14 again is typical for all the points that were monitored during the

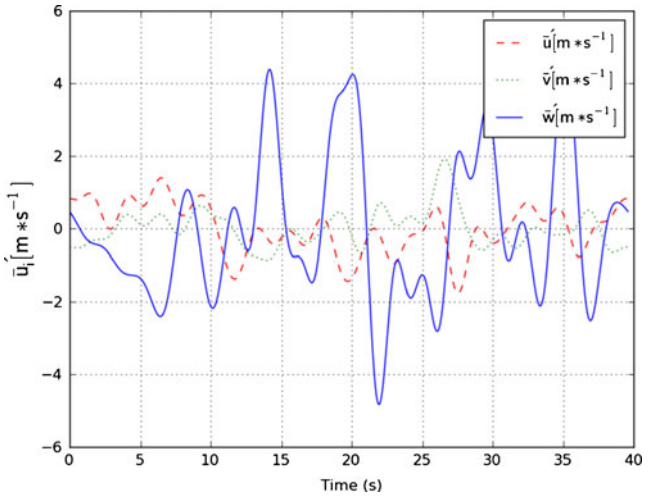

Fig. 13 Velocity fluctuations point 19, low pass filtered at 0.5 Hz (case: fine)

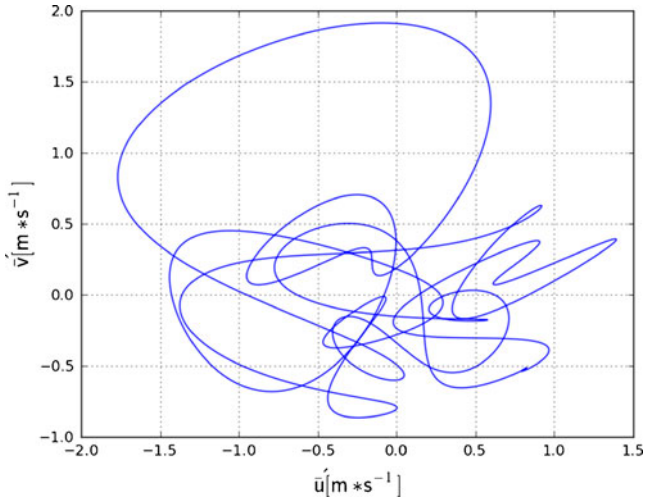

Fig. 14 Phase space plot of velocity fluctuations v' vs w', point 19, low pass filtered at 0.5 Hz (case: fine)

simulations. Current results indicate that the flow in the system studied exhibits complex precession.

4 Conclusions

Large-scale flow structures in a semi-industrial scale spray dryer were studied by LES. Convergence of the simulations was demonstrated by a grid and time step refinement study and the comparison of time step and cell size to estimates of the Kolmogorov time and length scales. The symmetry observed in the averaged fields of velocity magnitude and turbulence kinetic energy indicated that the simulation time was sufficient to capture slow moving flow modes.

Visual inspections of animations of the velocity field revealed that there are indeed large-scale flow structures that are transient in nature. The most pronounced transient structure that could be observed was the deflection of the jet towards the wall, especially in the lower conical part of the spray dryer. A deflection of the jet towards one position of the wall was observed to be often accompanied by gusts of upward-directed flow. The upward flowing gusts along the spray dryer wall from time to time extended from half the height of the cone section up to the spray dryer roof. In the averaged velocity field the gusts appeared, smaller in size and magnitude but still with upward velocity.

In the literature, no specific experimental data of systems resembling the current case more closely was found. However, based on extrapolation of the behaviour of confined jet flows, as summarised in the form of a regime map (Guo et al. 2001b), depicting flow modes, regular precession of the jet was expected. In contrast, neither the power spectra of the velocity fluctuations nor phase space plots of the cross-sectional velocities revealed periodic or regular behaviour. Instead, the jet movements were found to be complex and chaotic.

References

Davidson L (2010) How to estimate the resolution of an LES of recirculating flow. In: Quality and reliability of large-eddy simulations II. Springer: New York

Dellenback PA, Metzger DE, Neitzel GP (1988) Measurement in turbulent swirling flow through an abrupt axisymmetric expansion. AIAA J 26:669–681

Fletcher DF, Langrish TAG (2009) Scale-adaptive simulation (SAS) modelling of a pilot-scale spray dryer. Chem Eng Res Des 87:1371–1378

Fletcher DF, Guo B, Harvie D, Langrish TAG, Nijdam J, Williams J (2006) What is important in the simulation of spray dryer performance and how do current CFD models perform? Appl Math Model 30:1281–1292

Godijn ZM, Southwell DB, Kockel TK, Langrish TAG (1999) Flow visualisation in a pilot-scale spray dryer with two-fluid atomisation. CHEMECA 99:265–270, Newcastle Australia

Guo B, Langrish TAG, Fletcher DF (1998) Time-dependent simulation of turbulent flows in axisymmetric sudden expansions. 13th Australasian Fluid Mechanics Conference Australia

Guo B, Langrisch TAG, Fletcher DF (2001a) Simulation of turbulent swirl flow in an axisymmetric sudden expansion. AIAA J 39:96–102

Guo B, Langrisch TAG, Fletcher DF (2001b) Numerical simulation of unsteady turbulent flow in axisymmetric sudden expansions. J of Fluids Eng 123:574–587

Guo B, Langrisch TAG, Fletcher DF (2001c) An assessment of turbulence models applied to the simulation of a two-dimensional submerged jet. Appl Math Model 25:635–653

Guo B, Langrisch TAG, Fletcher DF (2003) Simulation of gas flow instability in a spray dryer. Trans IChemE 81:631–638

Hallett WLH, Gunther R (1984) Flow and mixing in swirling flow in a sudden expansion. Can J Mech Eng 62:149–155

Kieviet FG, Van Raaij J, De Moor PPEA, Kerkhof PJAM (1997) Measurement and modelling of the air flow pattern in a pilot-plant spray dryer. Chem Eng Res Des 75:321–328

Southwell DB, Langrish TAG (2001) The effect of swirl on flow stability in spray dryers. Trans IChemE 79 (Part A):222–234

Usui H, Sano Y, Yanagimoto Y, Yamasaki Y (1985) Turbulent flow in a spray drying chamber. J Chem Eng Japan 18:243–247

Woo MW, Daud WRW, Mujumdar AS, Wu Z, Talib MZM, Tasirin SM (2009) Non-swirling steady and transient flow simulations in short-form spray dryers. Chem Prod Process Model 4:1–34